Journal of Applied Electrochemistry **31**: 461–468, 2001.

Composite electrodeposition of ultrafine γ-alumina particles in nickel matrices Part I: Citrate and chloride electrolytes

A.B. VIDRINE and E.J. PODLAHA*
Gordon and Mary Cain Department of Chemical Engineering, Louisiana State University, Baton Rouge, LA 70803, USA
*(*author for correspondence, e-mail: podlaha@che.lsu.edu)*

Received 9 June 2000; accepted in revised form 20 October 2000

Key words: composite electrodeposition, direct-current plating, nickel–γ-alumina, pulse-reverse plating

Abstract

Electrodeposition of nanocomposite γ-alumina–nickel was examined using citrate and chloride electrolytes with rotating cylinder electrodes. Ultrafine alumina was detected in the nickel matrices and was found to depend on the applied current density. The particle incorporation rate dependence on the applied d.c. current density varied for the different electrolytes. In the chloride baths, higher particle concentrations were found in the deposits plated at low current densities compared to higher values. However, the opposite trend was noted for the citrate electrolyte where an increase in particle deposit content was observed with an increase in applied current density. Additionally, the nickel anodic behaviour was examined in order to devise a pulse-reverse (PR) plating method. PR deposition lead to an enhancement in the γ-alumina deposit concentration compared to DC plating in chloride electrolytes.

1. Introduction

Electrodeposition is one method to produce metal matrix composite (MMC) thin films. An insoluble material is suspended in a conventional plating electrolyte and is captured in the growing metal film. The second-phase material can be powder, fibre or an encapsulated particle, and its incorporation rate is affected by several interrelated parameters: the electrolyte concentration of the metal ions and particles, pH, applied current density/potential, agitation, organic additives and particle size [1, 2].

A considerable number of literature studies cite the enhanced properties resulting from micrometre and submicrometre size alumina particles embedded in nickel compared to pure nickel [3–9]. For example, microhardness, yield strength, tensile strength, and wear resistance are all improved by the presence of alumina in a nickel matrix. Microhardness of Ni–Al_2O_3 MMCs can be as much as two times that of pure nickel and increases with increasing alumina concentration and with decreasing particle size [3]. Yield and tensile strength increase as much as four times with the incorporation of alumina [4, 5]. In addition, Chang et al. [7] have determined that the increase in alumina concentration within the nickel matrix increased the MMCs wear resistance.

The recent availability of ever decreasing particle sizes has expanded potential MMC applications. Submicron size particles dispersed into a metal matrix not only promote homogeneity of the composite due to the increase metal–particle contact surface area, but would be a necessity for use as composite materials in microdevices. Since components of these devices are on the micron scale, the second-phase material in the metal matrix needs to be an order of magnitude smaller; thus, nanometric. Whereas particle size is known to influence its incorporation rate, the extent is still questionable. Several studies reported that the particle weight percent in a composite coating decreased as the particle diameter became smaller [6, 10, 11], while the opposite has also been observed [12]. The deposition rate of alumina into a nickel matrix, for example, has been found to decrease as the particle size becomes smaller [6], although in a separate study a much higher concentration of ultrafine alumina particles in nickel have been reported [13].

If the concentration of submicron particles embedded in the deposit under conventional DC plating is not sufficient, pulse reverse (PR) plating can be employed to eliminate a fraction of plated metal and thus increase the particle deposit concentration. The method has recently been demonstrated by Podlaha et al. [14] for the copper γ-alumina system, employing long, steady-state pulses, where the particle deposit concentration was improved six times over that found in DC electrodeposition. Conventional pulse-reverse plating has been employed by Kariapper et al. [15] with pulse lengths on the order of milliseconds, reporting no particle incorporation enhancement, but a loss of particle codeposition if the

pulse length is too rapid. Pulse plating, without an anodic component, has also been reported by Chen et al. [16] with rapid pulses. A moderate increase in particle deposit concentration was noted, coupled with a change in the surface microstructure.

In this study, the codeposition of nanometric size γ-alumina spherical particles in a nickel matrix is examined from different electrolytes. It is expected that the applied current density and electrode rotation rate will influence the particle deposition rate. The adaptability of the PR method to the nickel matrix requires the avoidance of passivating films and nonuniform dissolution, common to many nickel plating baths [17]. Thus, the dissolution behaviour of Ni in the composite plating electrolyte is examined. Different electrolytes are considered and the applied current density is varied under controlled hydrodynamic conditions. DC plating is compared with PR plating that consists of long pulses on the order of seconds to minutes.

2. Experimental details

A recessed, rotating cylinder electrode (RRCE) was used as the working electrode. The cylindrical electrodes measured 1.0 cm (0.39 in) in diameter by 1.2 cm (0.47 in) long and had a surface area of 3.77 cm^2 (0.58 in^2). The working electrode material was either Cu or 304 stainless steel plated with approximately 1 μm Au (Acid Gold Strike and Orotemp 24 Gold Solution by Technic Inc.). The gold surface was used for dissolution experiments and for improved deposit adhesion.

The rotation rate was controlled during each deposition in the turbulent flow regime. Values ranging from 1600 rpm ($Re = 4190$) to 225 rpm ($Re = 590$) were used. A stir bar located at the bottom of the cell kept the particles uniformly suspended in the solution. Care was taken so that the rotating electrode hydrodynamics, controlled by the rotation rate, was dominant compared to the agitation of the stir bar at the bottom of the cell.

A stationary nickel sheet (99.7% Ni) was used as the counter electrode and placed at a distance of 25 mm (1 in) away from the working electrode surface. A saturated calomel electrode (SCE) was used as the reference electrode. All experiments were performed at room temperature.

Three different electrolytes were studied: one citrate and two chloride based solutions. Their compositions are listed in Table 1. These baths are common for nickel electroplating and are examined here in order to establish their utility for nanocomposite electrodeposition. In all electrolytes examined, nanometric γ-Al_2O_3 particles (Nanophase Technologies Corporation, Il) were used. The averaged particle diameter reported by the manufacturer was 32 nm, having a specific surface area of 52 $m^2\ g^{-1}$. The pH was adjusted with H_2SO_4 or HCl, depending on the electrolyte type, before each plating experiment.

Table 1. Electrolytes

Bath	Constituents
Citrate bath	Variable $NiSO_4 \cdot 6H_2O$ 0.3 M $Na_3C_6H_5O_7 \cdot 2H_2O$ 25 g l^{-1} γ-Al_2O_3 pH 4.0
Chloride bath 1	0.71 M $(H_2NSO_3)Ni \cdot 4H_2O$ 0.063 M $NiCl_2$ 0.48 M H_3BO_3 25 g l^{-1} γ-Al_2O_3 pH 4.0
Chloride bath 2	0.2 M $NiCl_2 \cdot 6H_2O$ 0.4 M H_3BO_3 0.43 M NaCl 10 g l^{-1} γ-Al_2O_3 pH 3.0, 4.5

Direct current (DC) plating was carried out galvanostatically with an EG&G Princeton Applied Research potentiostat/galvanostat (model 363). A Zahner IM6 potentiostat/galvanostat system was used to produce polarization curves. The scan rate used for the polarization curves was 5 mV s^{-1}. Pulse-reverse (PR) plating was carried out using the EG&G Princeton Applied Research potentiostat/galvanostat (model 363) and an EG&G Parc Universal Programmer (model 175) function generator.

The concentration of aluminum (± 0.01 wt %) was analysed with a WDS electron microprobe (Superprobe 733, Jeol). Five to eight equidistant data points were measured and averaged. The dispersion in the data was typically 2–3% of the value. The alumina concentration was determined by using the aluminum to oxygen ratio of 2 to 3 defined by the chemical formula Al_2O_3. The current efficiency was calculated by Faraday's law based on the measured nickel concentration in the deposit and the total deposit mass (± 0.0001 g). The deposit thickness ranged from 1 to 16 μm (0.006 to 0.113 g). Reproducibility was confirmed with duplicate samples.

An environmental scanning electron microscope (ESEM 3, Electroscan) and a scanning electron microscope (Jeol, JSM-840A) was used to observe and compare the surface microstructure of the DC and PR deposits.

3. Results and discussion

3.1. *Citrate Bath*

Due to the earlier success of a copper–γ-alumina citrate plating bath [14] a similar electrolyte was chosen in this study. A direct substitution of 0.25 M copper sulphate from the previous study with nickel sulphate at the same pH resulted in an extremely low current efficiency as shown in Figure 1. The low current efficiency can be explained by the more negative deposition potential of nickel citrate compared to copper citrate. An increase in

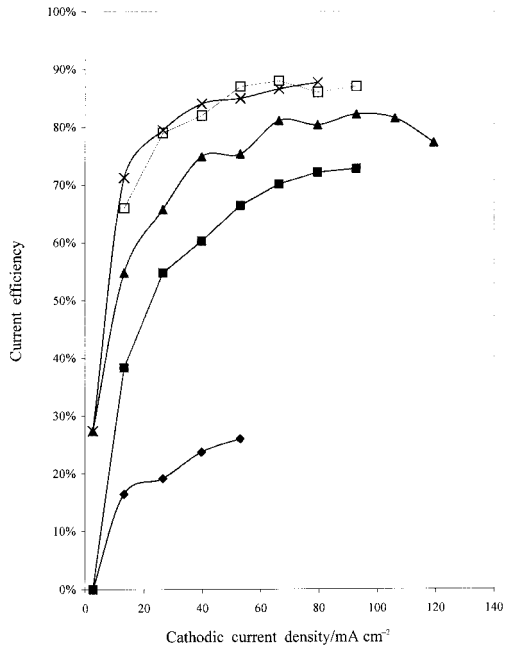

Fig. 1. Current efficiency measured for DC plating of nickel and nickel–γ-Al_2O_3, at a rotation rate of 1600 rpm; 0.3 M sodium citrate, pH 4.0. Nickel sulfate: (◆) 0.25 M, (■) 0.5 M, (▲) 0.7 M, (×) 1 M and (□) 1 M + 25 g l^{-1} alumina.

the nickel ion concentration resulted in a higher current efficiency. The addition of nickel sulfate at a constant citrate concentration generates more nickelous species available for reaction compared to the complexed nickel citrate species. The uncomplexed nickelous species reaction is more facile and occurs at a more noble potential than the complexed nickel reaction [18]. Thus, the largest current efficiency observed occurred when the total nickel ion concentration was 1.0 M and the citrate concentration was 0.3 M.

Addition of alumina particles to the concentrated nickel electrolyte had about the same current efficiency as the particle free solution. The concentration of alumina detected in the deposits is shown in Table 2 at 1600 rpm. The particle concentration was between 0.14 and 1.03 wt % Al_2O_3. Lower current densities favoured a low particle concentration with an increase in alumina concentration at the higher current densities.

The deposits had a dull gray colour with a matte finish. Figure 2 shows a SEM micrograph of the surface area of a typical composite plated from the citrate

Table 2. γ-Al_2O_3 deposit concentration DC plated from the citrate bath at 1600 rpm

$-i$ /mA cm^{-2}	γ-Al_2O_3 /wt %
13.3, 26.5	0
39.8	0.14
53.1	0.35
66.3	0.26
79.6	1.03
92.8	1.01

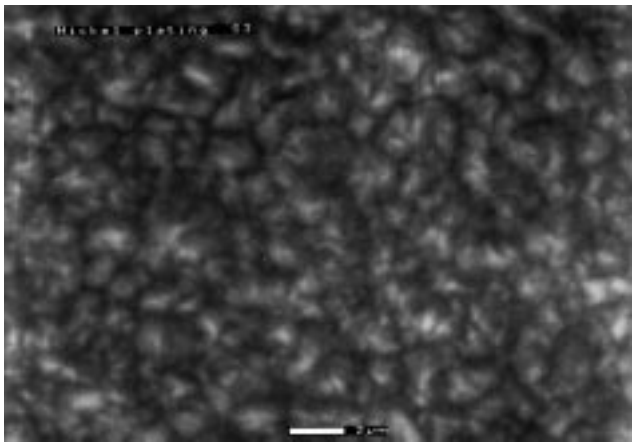

Fig. 2. SEM micrograph of a 0.26 wt % γ-Al_2O_3–nickel composite from the citrate bath.

electrolyte. A nodular microstructure was observed with no pitting or cracks detected when magnified 5000×.

Although satisfactory DC electrodeposition was possible from the citrate electrolyte, a satisfactory dissolution condition was not found. The anodic dissolution of nickel was not obtainable with any of the sodium citrate solutions. The anodic polarization curve for the citrate solution with 1 M nickel sulfate is shown in Figure 3. A distinct passive region is observed between 0.2 and 1.2 V vs SCE. The apparent transpassive region (beginning at about 1.2 V) was not indicative of nickel dissolution, as verified with constant current electrolysis, and therefore represents the onset of oxygen evolution. In the apparent active region at potentials more noble than 0.15 V, dissolution of the composite was not observed. Since this bath did not allow for nickel dissolution, pulse-reverse plating would not be effective. Therefore, the chloride electrolytes were considered.

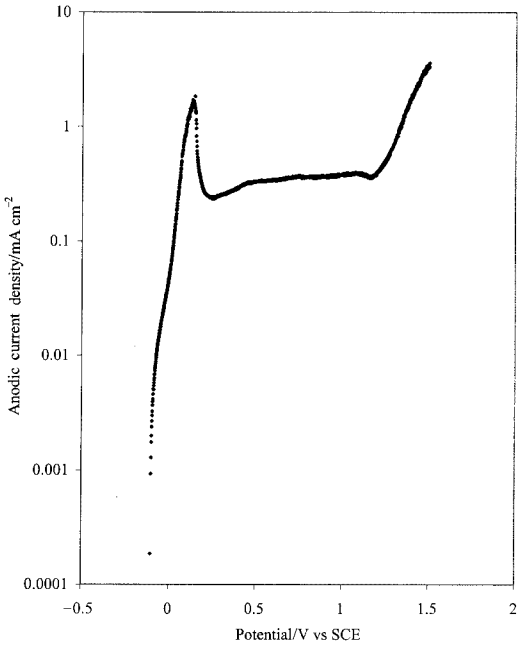

Fig. 3. Anodic polarization of the 1.0 m nickel sulphate–citrate electrolyte with 25 g l^{-1} alumina at a rotation rate of 1600 rpm.

3.2. *Chloride baths*

The two chloride electrolytes listed in Table 1 were adapted from the literature. Chan et al. [19–21] successfully pulse-reverse electroplated pure nickel using a nickel chloride–sulphamate electrolyte. The bath used here was modified slightly from that used by Chan et al. by the addition of alumina particles and is designated as chloride bath 1. Webb et al. [13], on the other hand, have shown that high concentrations of nanometric alumina particles in nickel can be codeposited under DC plating conditions onto a rotating disk electrode (RDE) from a chloride-boric acid solution. Their electrolyte contained no sulphamate. Also, a considerably lower amount of nickel ion concentration was used by Webb et al. than by Chan et al. Therefore the particle concentration was lowered to have a more comparable nickel/particle electrolyte concentration and to match the same particle electrolyte concentration as reported by Webb et al. This bath is denoted as chloride bath 2.

3.2.1. *Anodic polarization behaviour*

To determine if PR plating would be possible the anodic polarization behaviour of chloride bath 1 was examined. Figure 4 shows the anodic polarization curve carried out on a DC plated nickel sample. A characteristic passive region is not evident, which is desirable for defining a wide range of PR plating operating conditions. In addition, the anodic polarization is largely affected by the presence of particles. Without the addition of particles the dissolution current is lower and typical passive regions are evident (see Figure 4). The anodic polarization curve of the other chloride electrolyte, chloride bath 2, with particle addition, is shown in Figure 5. A narrow passive region is observed, but is followed by a transpassive region that allowed for the anodic dissolution of nickel as determined by constant current dissolution experiments in this potential range. The passive to transpassive region depended on pH, as illustrated for pH 3 and 4.5.

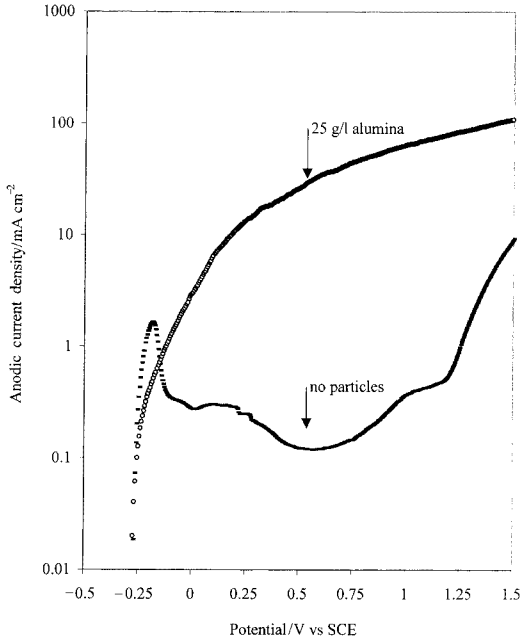

Fig. 4. Anodic polarization of the chloride bath 1 containing nickel sulfamate with and without particles at a rotation rate of 1600 rpm.

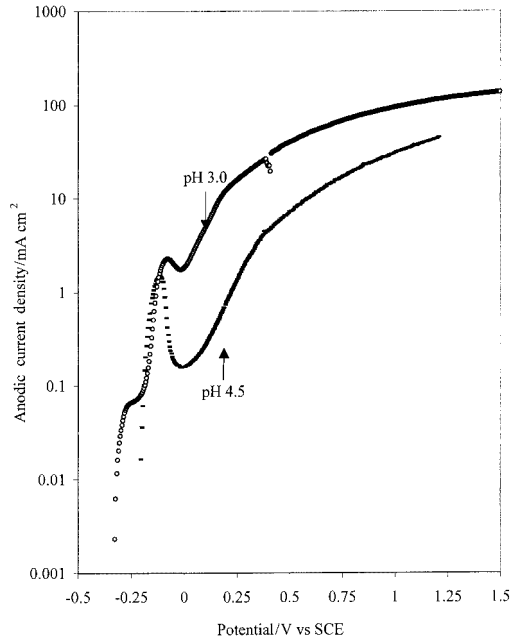

Fig. 5. Anodic polarization of the chloride bath 2 containing nickel sulfamate with particles at a rotation rate of 1600 rpm at two different pH units.

3.2.2. *DC deposition*

The weight percent alumina detected in the deposit from chloride bath 1 is presented in Figure 6 at a constant

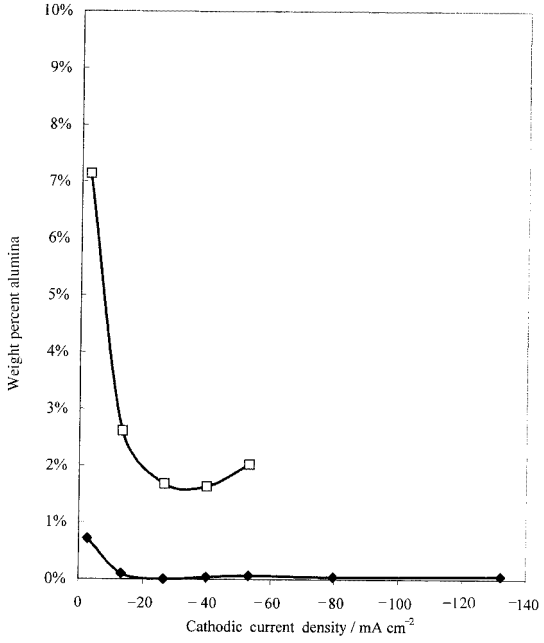

Fig. 6. Weight percent alumina of deposits DC plated from chloride bath 1 containing nickel sulfamate with an electrode rotation rate of 1600 rpm (◆) and 225 rpm (□).

Table 3. γ-Al_2O_3 deposit concentration DC plated from chloride bath 2 at 1600 rpm

$-i$ /mA cm^{-2}	γ-Al_2O_3 /wt %	Efficiency /%
39.8	1.18	92.3
53.1	0.05	92.9
66.3	0.02	92.2
79.6	0.01	93.1
92.8	0.1	96.4

rotation rate of 1600 and 225 rpm. The low rotation rate favoured particle incorporation at all applied current densities. The highest particle incorporation occurred at the lowest applied current density of −2.7 mA cm^{-2}. Compared to the citrate electrolyte at the same rotation rate of 1600 rpm, the particle incorporation extent is about the same, however, the incorporation rate dependence on the applied current is different. The highest particle deposit concentrations are found at a low current density (−2.7 mA cm^{-2}) for chloride bath 1 and decrease with applied current. The citrate electrolyte shows the opposite behaviour with a comparable particle weight percentage achieved only at a much higher current density (>80 mA cm^{-2}). For the citrate bath, an increase in the applied current density lead to an increase in the particle deposit concentration.

Chloride bath 2 at pH 3 revealed a similar particle incorporation behaviour as chloride bath 1. Table 3 shows the weight percent particle incorporation as a function of applied current density from chloride bath 2 at 1600 rpm. As the cathodic current density increased the particle concentration in the deposit diminished.

Figure 7 shows the current efficiency of the composites DC plated at 1600 and 225 rpm from chloride bath

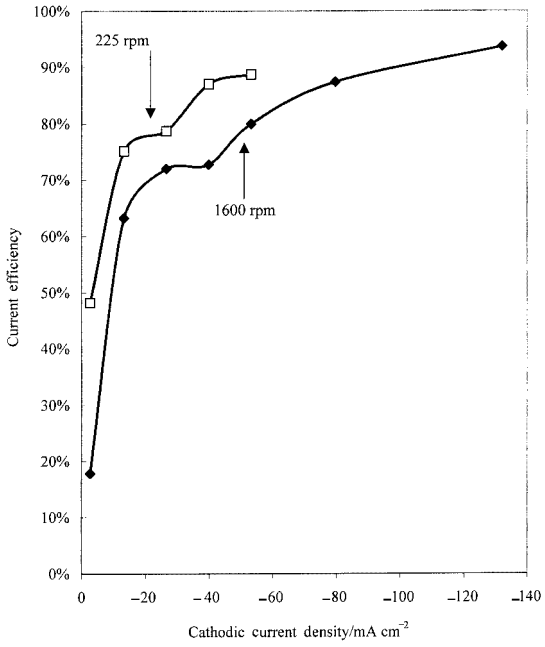

Fig. 7. Current efficiency of deposits DC plated from chloride bath 1 containing nickel sulfamate with an electrode rotation rate of 1600 rpm and 225 rpm.

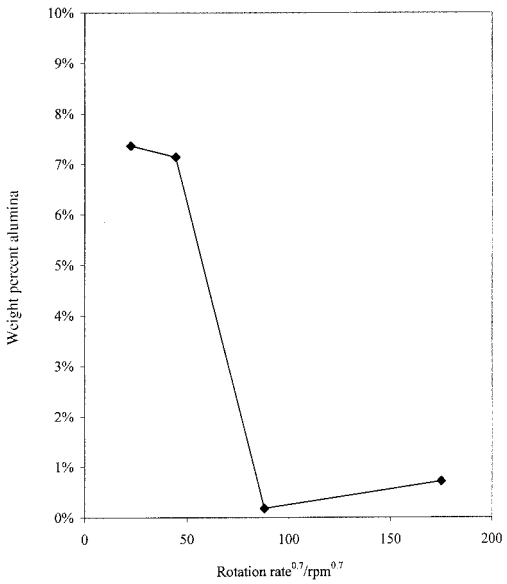

Fig. 8. Weight percent alumina of deposits DC plated from chloride bath 1 containing nickel sulfamate with a variation of electrode rotation rate at an applied cathodic current density of −2.7 mA cm^{-2}.

1. For both rotation rates, the current efficiency varies greatly, with an overall improvement at the low rotation rate. The high particle incorporation extent occurs where the current efficiency is lowest. Therefore, when comparing the chloride bath 1 to the citrate bath with a similar rotation rate (1600 rpm), it is the citrate bath that is superior due to a considerably higher current efficiency (see Figure 1, Table 2) when the particle deposit concentration is the same. Comparing the two chloride electrolytes, it is chloride bath 2 that has a higher current efficiency. Table 3 shows that the current efficiency is above 90% for all applied current densities studied in chloride bath 2 and is slightly greater than that found for the citrate electrolyte.

As suggested in Figure 6 there is a strong influence of rotation rate on particle incorporation, particularly at low current densities. Figure 8 shows the deposit particle concentration at a constant applied current of −2.7 mA cm^{-2} for deposits DC plated from the chloride bath 1. The very low applied current density is far below the nickel reduction limiting current density, and is therefore not influenced by the variation in rotation rate. The large increase in particle concentration at low rotation rates does not follow a 0.7 power relation as predicted for mass transport controlled species deposited onto a rotating cylinder electrode [22]. This suggests that shearing and adsorption forces must be rate controlling. Thus, an increase in rotation rate increases the shear forces acting on the particle and results in a lower particle deposit concentration.

3.2.3. *PR deposition*

The conditions chosen for pulse-reverse plating were 225 rpm and ±26.5 mA cm^{-2} using chloride bath 1 containing sulfamate. A current density of −26.5 mA cm^{-2} was chosen as the cathodic plating current density because a

compromise was made between alumina incorporation and current efficiency. An anodic current density of $+26.5$ mA cm^{-2} was used due to the smooth surface morphology obtained during dissolution. Two types of PR experiments were performed. In one set of experiments, the anodic dissolution time, t_a, was held constant while varying the cathodic plating time, t_c. In another set of experiments the cathodic plating time was constant and the anodic dissolution time was varied. The total deposition charge, $Q_t = (|Q_c| - |Q_a|)N$, was constant at 10.6 C cm^{-2}, where Q_c and Q_a are the cathodic and anodic charges, respectively, and N is the number of cycles.

The deposit particle concentration and current efficiency results are shown in Figures 9 and 10, respectively, as a function of duty cycle. Duty cycle is defined as

$$\text{Duty cycle} = \frac{|Q_c| - |Q_a|}{|Q_c|}$$

A duty cycle of 1.0 corresponds to DC plating. While holding t_a constant at 5 s, deposits were only obtainable at duty cycles of 0.8 or larger. No deposits could be obtained below a duty cycle of 0.8 because they were nonadherent and cracked. Generally, the PR plating

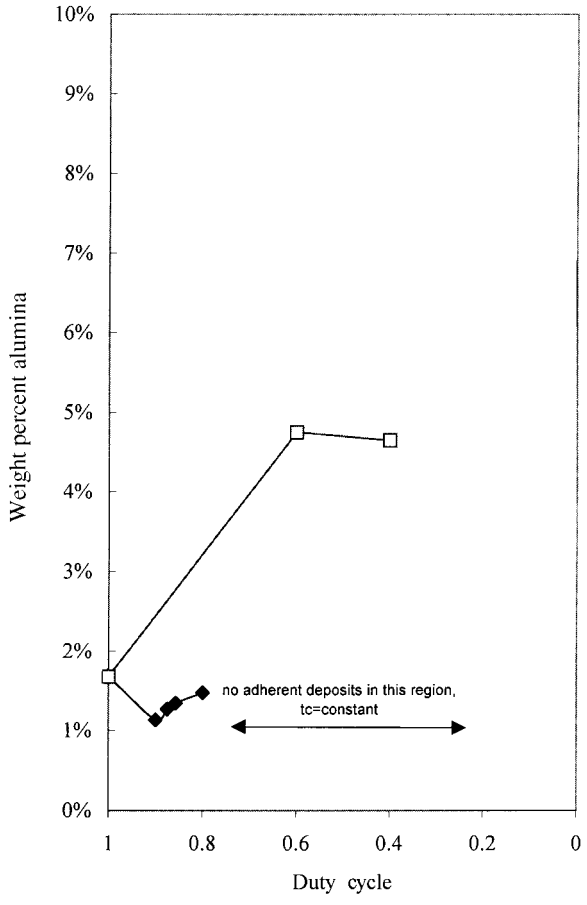

Fig. 9. Weight percent alumina of deposits PR plated from chloride bath 1 during PR plating at a rotation rate of 225 rpm. Key: (◆) t_a = constant; (□) t_c = constant.

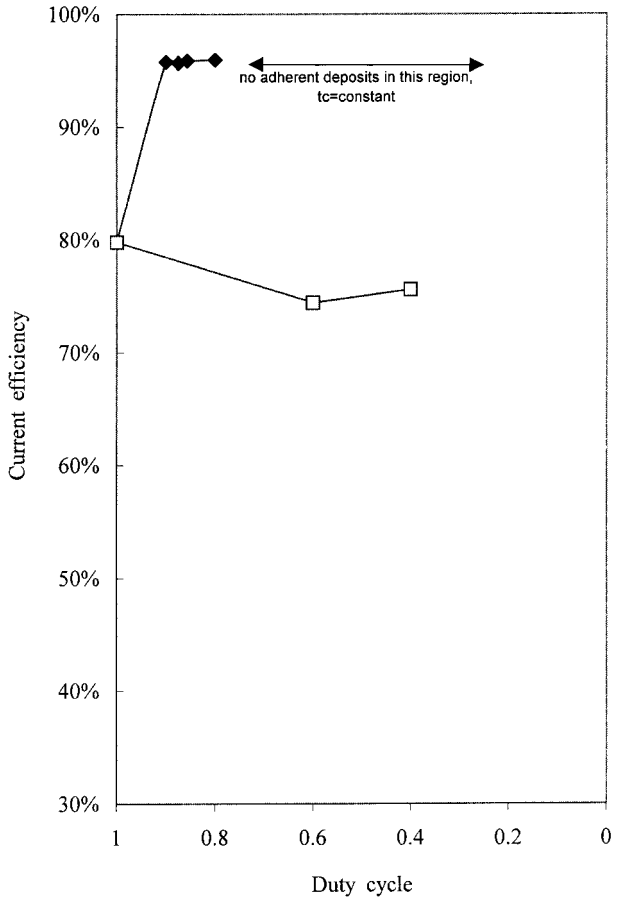

Fig. 10. Current efficiency determined for chloride bath 1 during PR plating at a rotation rate of 225 rpm. Key: (◆) t_a = constant; (□) t_c = constant.

increased the cathodic current efficiency. PR plating did not significantly influence the incorporation of alumina.

While holding t_c constant at 25 s, the current efficiency decreased slightly from 80% to 75%, as a function of duty cycle. However, an increase in alumina deposit incorporation occurred. At a duty cycle of 0.4 the increase in alumina from went from 1.68% for DC plating to 4.7%. These PR deposits were rough with a dull gray colour and matte finish.

Figure 11 compares the surface morphology of the PR (duty cycle of 0.8) and DC deposits produced with chloride bath 1. PR plating changed slightly the microstructure of the MMC. The nodular surface is apparent in both micrographs, but the PR deposit contains larger nodules than the DC deposit, consistent with a smoother surface morphology.

The second chloride bath containing no sulphamate, chloride bath 2, was also used to investigate PR plating. The anodic condition used for the pulse-reverse method was chosen in order to optimize the rate while maintaining smooth deposit morphology. The pH 3.0 chloride bath was first tested using varied combinations of cathodic and anodic current densities and times, no adherent deposits were produced. They were severely cracked and pitted; due presumably to passivated films mixed in with the deposit matrix. The pH 4.5 chloride

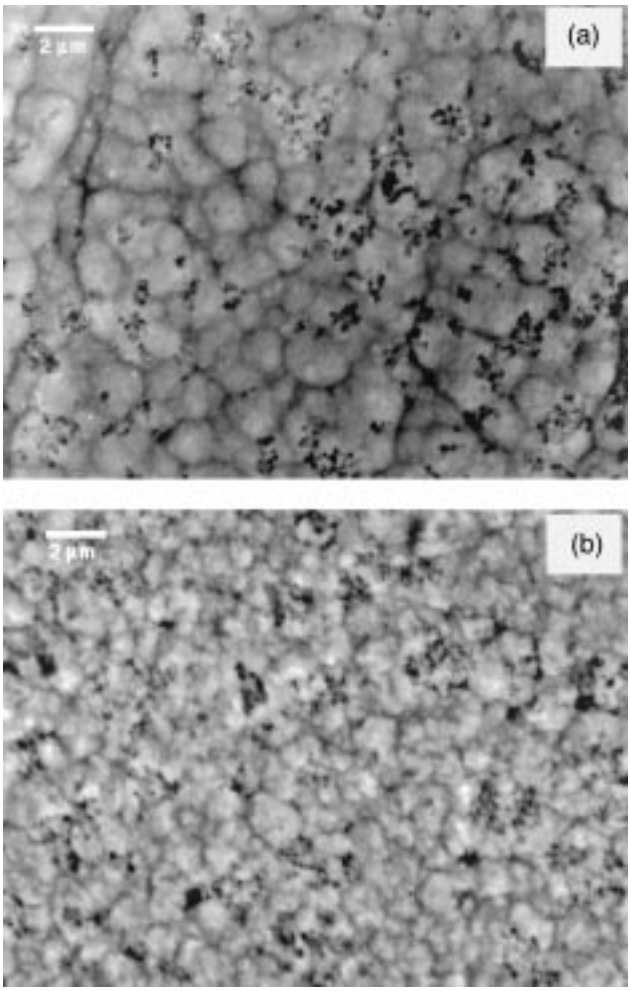

Fig. 11. SEM micrograph of a γ-Al_2O_3 – copper composite from for chloride bath 1, (a) PR conditions: $i_c = -26.5$ mA cm^{-2}, $i_a = 26.5$ mA cm^{-2}, $t_c = 25$ s, $t_a = 5$ s, duty cycle = 0.8, (b) DC conditions: $i_c = -26.5$ mA cm^{-2}, $t_c = 6$ min and 40 s, at a rotation rate of 225 rpm.

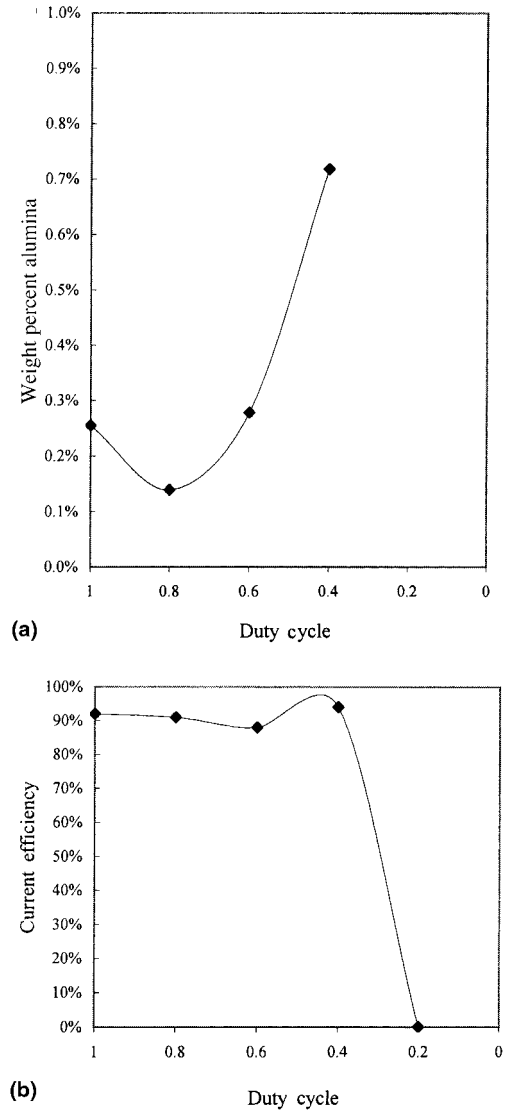

Fig. 12. (a) Weight percent alumina and (b) current efficiency of deposits PR plated from chloride bath 2 during PR plating at a rotation rate of 1600 rpm, pH 4.5.

bath proved more promising. The anodic condition used for the pulse-reverse method was chosen in order to optimize the rate while maintaining smooth deposit morphology. Anodizing at $+39.8$ mA cm^{-2} was considered a fair compromise. The cathodic deposition time was constant and the anodic dissolution time varied. The total plating charge, Q_t, was 50 C cm^{-2}. The rotation rate was held constant at 1600 rpm. The alumina deposit concentration and current efficiency is shown in Figure 12. The alumina concentration in the nickel matrix increased nearly three times greater than the DC plated deposit at a duty cycle of 0.4. Current efficiencies near 90% were achieved for PR deposits having duty cycles between 0.8 and 0.4. A lower duty cycle of 0.2 resulted in poorly adhered deposits that did not appear completely metallic.

The adherent PR plated deposits, however, exhibited a nonuniform morphology. Figure 13 compares the DC plated sample with the 0.4 duty cycle PR plated sample from chloride bath 2. Pits and cracks were evident on the PR sample when magnified 500× as shown in the SEM micrographs. The nodular structure is apparent in both micrographs; the DC plating produced a finer nodular surface than the PR plating.

4. Conclusions

Ultrafine γ-alumina particles were incorporated into a nickel matrix in both citrate and chloride electrolytes. Particle deposit concentration decreased with applied current density for the chloride baths but increased for the citrate bath. The current efficiency improved with an increase in applied current density for all electrolytes. Therefore, the citrate electrolyte is most attractive for further optimizing particle incorporation and deposition time for DC electrodeposition. Particle incorporation is also greatly affected by the electrode rotation rate and by pulse-reverse plating. Pulse-reverse plating was carried out with the chloride electrolytes and lead to an enhancement in the γ-alumina deposit concentration

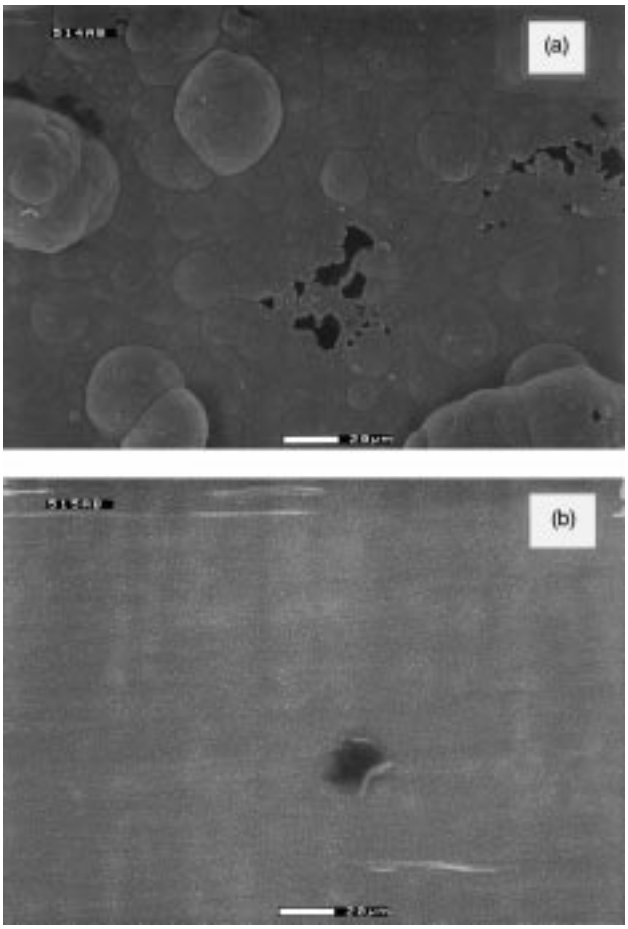

Fig. 13. SEM micrograph of a γ-Al_2O_3–copper composite from chloride bath 2 (a) PR conditions were: $i_c = -39.0$ mA cm^{-2}, $i_a = 39.8$ mA cm^{-2}, $t_c = 25$ s, $t_a = 15$ s, duty cycle = 0.4, (b) DC conditions were: $i_c = -39.8$ mA cm^{-2}, $t_c = 20$ min, at pH 4.5 and a rotation rate of 1600 rpm.

compared to DC plating under the same conditions. PR deposits had larger nodular microstructures than DC plated deposits. Adequate dissolution conditions were not found with the citrate electrolyte due to the formation of a passivated surface and therefore pulse-reverse plating was not attempted from this solution.

Acknowledgements

Support of this work was provided in part by AESF and by a Shell Faculty Career Initiation Fund. The aid of Dr Xie and Dr G. Griffin is warmly acknowledged for their help in the microstructure analysis.

References

1. A. Hovestad and L.J.J. Janssen, *J. Appl. Electrochem.* **25** (1995) 519.
2. R. Narayan and B.H. Narayana, *in* J. Yahalom (Ed), 'Reviews on Coatings and Corrosion', Vol. 4(1), Freund Publishing House, Tel-Aviv, Israel, (1979).
3. V.P. Greco and W. Baldauf, *Plating* **55** (1968) 250.
4. V.O. Nwoko and L.L. Shreir, *J. Appl. Electrochem.* **3** (1973) 137.
5. F.K. Sautter, *J. Electrochem. Soc.* **110** (1963) 557.
6. E.A. Brandes and D. Goldthorpe, *Metallurgia* **76** (1967) 195.
7. Y.-S. Chang and J.-Y. Lee, *Mater. Chem. Phys.* **20** (1988) 309.
8. M. Verelst, J.P. Bonino, M. Brieu and A. Rousset, *Mater. Sci. Eng.* **A191** (1995) 165.
9. M. Verelst, J.P. Bonino and A. Rousset, *Mater. Sci. Eng.* **A135** (1991) 51.
10. G. Maurin and A. Lavanant, *J. Appl. Electrochem.* **25** (1995) 1113.
11. R. Bazard and P.J. Boden, *Trans. Inst. Met. Finish.* **50** (1972) 63.
12. Y. Suzuki and O. Asai, *J. Electrochem. Soc.* **134** (1987) 1905.
13. P. Webb and N. Robertson, *J. Electrochem. Soc.* **141** (1994) 669.
14. E.J. Podlaha and D. Landolt, *J. Electrochem. Soc.* **144** (1997) L200.
15. A.M.J. Kariapper and J. Foster, *Trans. Inst. Met. Finish.* **52** (1974) 87.
16. E.S. Chen and F.K. Sautter, *Plat. Surf. Finish.* **63** (1976) 28.
17. G.A. DiBari, *Plat. Surf. Finish.* **86** (1999) 32.
18. Ch. Bonhote, E.J. Podlaha and D. Landolt, *Electrochim. Acta* **39** (1994) 2649.
19. K.C. Chan, N.S. Qu and D. Zhu, *J. Mat. Process. Technol.* **63** (1997) 819.
20. N.S. Qu, K.C. Chan and D. Zhu, *Plat. Surf. Finish.* **91** (1997) 220.
21. K.C. Chan, N.S. Qu and D. Zhu, *Surf. Coat. Technol.* **99** (1998) 69.
22. M. Eisenberg, C.W. Tobais and C.R. Wilke, *J. Electrochem. Soc.* **101** (1954) 306.